Conduction mechanisms and voltage drop during field electron emission from diamond needles

Olivier Torresin, Mario Borz, Julien Mauchain, Ivan Blum, Victor Kleshch, Alexander Obraztsov, Angela Vella, Benoît Chalopin

Version of Record: https://www.sciencedirect.com/science/article/pii/S0304399118303930
Manuscript_00f08235f62066024d827bf5bc1a43d8

Conduction mechanisms and voltage drop during field electron emission from diamond needles

Olivier Torresin,[1] Mario Borz,[2] Julien Mauchain,[1] Ivan Blum,[2] Victor I. Kleshch,[3] Alexander N. Obraztsov,[3,4] Angela Vella,[2] and Benoit Chalopin[1,*]

[1] *Laboratoire Collisions Agrégats Réactivité, Université de Toulouse, UPS, CNRS*
[2] *Groupe de Physique des Matériaux, Université de Rouen, INSA Rouen, CNRS*
[3] *Department of Physics, M.V. Lomonosov Moscow State University*
[4] *Department of Physics and Mathematics, University of Eastern Finland*

(Dated: February 4, 2019)

We report results of experimental investigation of field electron emission from diamond nanoemitters. The measurements were performed with single crystal diamond needles fixed at tungsten tips. The voltage drop along diamond needles during emission was revealed and measured using electron energy spectroscopy. The observed linear dependence of the voltage drop in diamond on voltage applied to the tungsten tip is explained in the frame of a simple macroscopic electrical model combining Poole-Frenkel conduction along the diamond tip and Fowler-Nordheim tunneling at the diamond-vacuum junction. Experimental evidences of electron emission sensitivity to laser illumination are discussed for possible modification of diamond emitter characteristics and voltage drop.

I. INTRODUCTION

Diamond attracted a lot of interest over the last decades as alternative to conductive metallic and semiconducting cold cathodes [1–9]. Attempts to build diamond-based and diamond-like emitter arrays, to function as field emission displays, were ultimately commercially unsuccessful, but the potential for using a diamond nanocrystal to act as a point-electron source was not systematically explored in this earlier work. High mechanical robustness, thermal conductivity and chemical inertness intrinsically possessed by diamond, could be key factors providing a desirable stability of electron source. Most studies with electric fields in the range of 1MV/m were performed previously on polycrystalline diamond films or composites of nanostructured diamond species with doped or defective diamond. Recently, Kleshch et al. [10] first demonstrated the use of a single-crystal diamond needle as a point electron source. One of their findings was a saturation phenomenon of electron emission manifested in deviation of current-voltage curve from the Fowler-Nordheim dependence at high voltages. The current in the saturation region follows a Poole-Frenkel mechanism and is associated to a voltage drop detected in the measurement of kinetic energy spectra of the emitted electrons. The formation of a depletion zone near the diamond tip apex, which is typical for semiconductor emitters [11], may happen in the saturation regime. This saturation of current may also be explained by a reduction of the field enhancement factor (see. e.g. [12]) because of a voltage drop along the emitter as it has also been observed by Groening et al. [7] for diamond films and discussed recently by Forbes [13]. He argues that this effective "saturation" of Fowler-Nordheim plots can come from a voltage-divider effect. This paper extends on that idea and investigates the conduction and emission properties of diamond needles (representing a kind of diamond nanoemitters), where the voltage drop is substantial. In the following, we present measurements of electron emission from a diamond nanotip which confirm and extend previous results obtained for similar diamond crystallites [10]. We use kinetic energy spectra of emitted electrons to characterize the conduction mechanisms as a combination of Poole-Frenkel conduction in the diamond and Fowler-Nordheim tunneling at the diamond-vacuum junction. At this stage in our investigation of electron emission from diamond needles, we focus on the experimental results revealing the main practical aspects of the emission and on the simplest modeling of the data from which general characteristics of the sample could be extracted. Even though some microscopic considerations will be discussed, the aim of this article is to get a macroscopic view on conduction mechanisms on this object but not to discuss the microscopic aspects of the electrons transport and the electric field distribution inside the diamond needle. Section II describes the diamond needles used in our experiment, section III presents the results of electron emission measurements, section IV describes an electrical model used to account for the two different conduction mechanisms, and section V shows the possibilities to control electron emission by laser illumination of the tip apex.

II. SINGLE-CRYSTAL DIAMOND NEEDLES

The diamond needles used in our experiments are (001) oriented single crystals, created by chemical vapor deposition (CVD) and selective thermal oxidation. The fabrication process is described in Ref. [14] and the needles have been investigated on several different aspects: in terms of structural properties [15], field emission [10], optical response in electron emission [16], photolumi-

* benoit.chalopin@irsamc.ups-tlse.fr

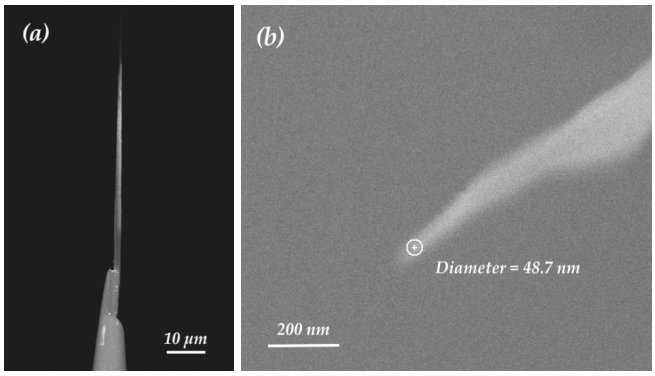

FIG. 1: SEM images of a single-crystal diamond needle mounted on a tungsten nanotip using FIB (a) and close-up on the apex (b) from which the radius is estimated.

nescence and cathodoluminescence [17–20]. They were welded on a tungsten nanotip using Focused Ion Beam (FIB). The diamond needles macroscopically have a pyramidal shape (while shape of near apex lost the geometrically perfect form), with a length of 50 to 100 μm, and a apex radius of 10 to 50 nm. This dimension is similar to a typical tungsten nanotip used for cold field emission, which justifies the comparison of their field emission properties. Several diamond needles have been used. The sample used in the experiment presented here is shown in Fig. 1

III. ELECTRON FIELD EMISSION

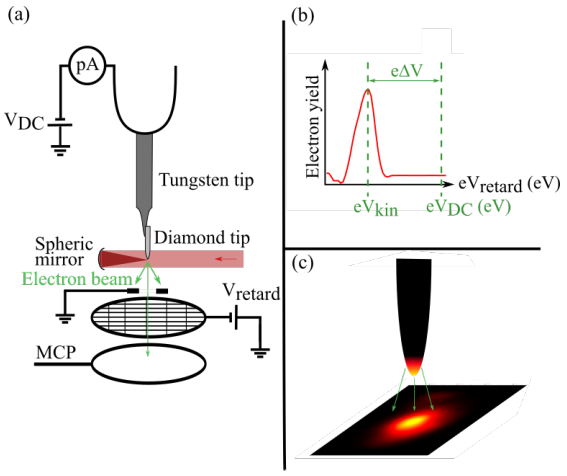

FIG. 2: (a) Experimental setup for electron emission investigation (see text for details). (b) Typical energy spectrum recorded by the retarding field spectrometer, from which the voltage drop ΔV is measured. (c) Typical field emission microscopy image.

Fig. 2(a) shows a sketch of the experimental apparatus for electron emission, adapted from [21, 22]. Diamond tips and their tungsten holder are mounted inside an ultra-high vacuum chamber designed for field and laser-induced electron emission with a pressure of 2×10^{-10} mbar. Tips are biased with a voltage V_{DC}. The total emitted current is measured with a picoammeter, plugged on the tip at high voltage and isolated from ground. This measurement comes with a noise of a few tens of pA. The electron kinetic energy spectrum is measured with a retarding field spectrometer at zero potential with an entrance pinhole of 200 μm, counting electrons with a multi-channel plate. The latter has a resolution of approximately 1 eV within our operating parameters. A typical spectrum is shown in Fig. 2(b) in which the width is limited by the low-resolution of the spectrometer. We can therefore not measure precisely the features of the spectrum but only the mean kinetic energy of the emitted electrons. The spectrometer is a few millimeters away from the tip apex and is mounted on translation stages in order to perform field-emission microscopy (FEM) (Fig. 2(c)). A femtosecond laser (wavelength $\lambda = 1030$ nm, 300 fs pulse duration, variable repetition rate from 1 kHz to 2 MHz) can be focused on the apex with a beam size of a few micrometres, allowing the illumination of the apex only. Taking into account the submicrometer transverse dimension of the needle near the apex, the laser beam power illuminating of the needle may be estimated as about 10% of the incident power.

Before they are used as electron sources, the needles are cleaned using a combination of the application of a 2.5 kV positive applied voltage for three minutes, and focused laser illumination for an hour with a mean power of a 120 mW. We observed that strong emission currents or high laser intensities can cause modification of the needles' shape and their emission properties. However with moderate currents and laser intensities, which were used in this work, no substantial damage was observed on the diamond needles. This corresponds to our expectations based on the high optical transparency of diamond in the visible range.

The kinetic energy of emitted electrons is not equal to eV_{DC} because of the voltage drop ΔV between both ends of the diamond needle. Since the voltage between the tip apex and the grounded counter-electrode is $V_{\mathrm{DC}} - \Delta V$, we write this energy as $E_{kin} = e(V_{\mathrm{DC}} - \Delta V)$ where e is the elementary positive charge.

We measured the field-emission current as well as the voltage drop ΔV as a function of the applied voltage V_{DC} (Fig. 3) using the picoampermeter and the spectrometer. The current rises exponentially and we reach currents of a few nA for applied voltage between 400 V and 1.5 kV. The picoammeter has a resolution of about 10 pA. Hence, we were not able to measure current below 100 pA which corresponds to applied voltage below 400V. At these currents we observed substantial voltage drop of several hundreds of volts, similarly to previously reported results [10] which were obtained in the current saturation region. The voltage drop however behaves linearly as a

function of the applied voltage V_{DC} with a non-zero intercept of $-134\,\mathrm{V}$ and a slope of 0.53.

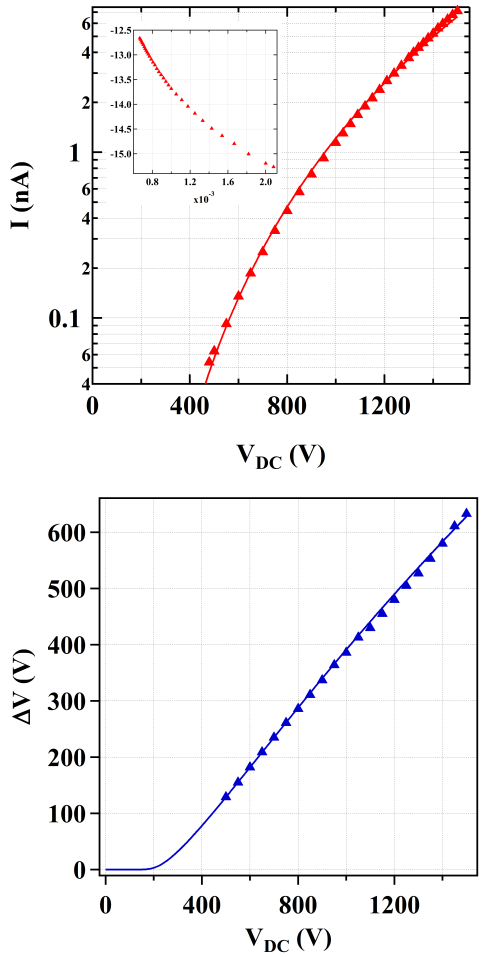

FIG. 3: Top: Measured current I as a function of the applied voltage V_{DC} (triangles) in semilog scale. In solid lines is the computed value resulting from equation 3 using parameters from the fits of equations 1 and 2. Inset shows a current versus V_{DC} in usual FN coordinates $\ln\left(\frac{I}{V_{\mathrm{DC}}^2}\right)$ versus $\frac{1}{V_{\mathrm{DC}}}$. Bottom: Measurement of the voltage drop ΔV as a function of V_{DC} (triangles) and corresponding computed value from equation 3 (solid line).

IV. CONDUCTION MODEL FOR ELECTRONS

To explain the evolution of the current and the voltage drop as a function of the applied voltage, we introduce a simple macroscopic electrical model for the conduction of electrons between the tungsten holder and the spectrometer. This macroscopic model aims at explaining the dependence of current and voltage drop as a function of applied voltage. Two conduction mechanisms are simultaneously happening. We model them as differential

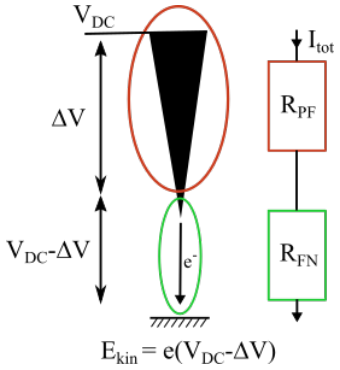

FIG. 4: Conduction model for the emission current: the Poole-Frenkel and Fowler-Nordheim dipoles are in serial so that the emission current should obey both the Poole-Frenkel and Fowler-Nordheim laws with a corresponding potentiel difference ΔV and $(V_{\mathrm{DC}} - \Delta V)$ respectively.

resistances connected in series with the same electrical current I (Fig. 4). First in the diamond, the conduction in the saturation region is best described with the Poole-Frenkel mechanism [10, 23–25] associated with a voltage ΔV which scales as :

$$I = A\,\Delta V\, e^{B\sqrt{\Delta V}} \tag{1}$$

where A and B are constants depending on the tip characteristics and temperature (described later). This mechanism can be understood as thermally stimulated emission of charges over a potential-energy barrier reduced by the Schottky effect. It is important to notice here that this macroscopic point of view can apply to both surface conduction and bulk conduction. Although a microscopic description of the conduction could provide a better understanding of the role of the various parameters, the macroscopic model we use here is proving sufficient to model the experimental data. Then at the diamond-vacuum junction, electrons are emitted through field emission, with a Fowler-Nordheim behaviour [26–28] associated to a local electrostatic field of magnitude E_{FN}. As in the case for cold field emission from metallic nanotips, we can link this electric field to the potential at the tip apex. But in this case, the potential at the tip apex differs from the applied voltage V_{DC} by the voltage drop. Hence, in the same spirit as for conductive emitters, we can write $E_{FN} = \beta(V_{\mathrm{DC}} - \Delta V)$. β (in m^{-1}) is a parameter that describes field enhancement at the tip apex. In the following, we make the assumption that β is constant and does not depend on V_{DC} or ΔV. This strong hypothesis is an approximation because of a possible field penetration to the emitter tip, especially when the depletion region is formed [24, 29], as well as because of the non linearity of PF conduction. This non-linearity makes the field profile in diamond non-homogenous, and the shape of the iso-potential lines at the apex (which β depends on) should therefore depend on the applied voltage or current. A more detailed microscopic analysis

of the field profile versus PF current would be necessary to determine the exact dependance with the applied voltage. But this is outside the scope of this article and from there on, we consider β to be constant. We can therefore write:

$$I = C(V_{\mathrm{DC}} - \Delta V)^2\, e^{-\frac{D}{V_{\mathrm{DC}}-\Delta V}} \qquad (2)$$

where C and $D \propto \phi^{3/2}/\beta$ are approximately constants depending on the workfunction ϕ and the voltage-to-field β factor.Considering that the PF and FN currents must be equal in the static regime, we write:

$$I = A\,\Delta V\, e^{B\sqrt{\Delta V}} = C(V_{\mathrm{DC}} - \Delta V)^2\, e^{-\frac{D}{V_{\mathrm{DC}}-\Delta V}} \qquad (3)$$

Using equations (1) and (2), we can fit the current using both the PF ($\ln\frac{I}{\Delta V}$ vs ΔV) and FN ($\ln\frac{I}{(V_{\mathrm{DC}}-\Delta V)^2}$ vs $\frac{1}{V_{\mathrm{DC}}-\Delta V}$) coordinates as shown in Fig. 5. The PF fit gives $A_0 = 3.04 \pm 0.03 \times 10^{-5}\,\mathrm{nA/V}$ and $B_0 = 0.239 \pm 0.001\,\mathrm{V}^{-1/2}$, and the FN fit gives $C_0 = 7.49 \pm 0.09 \times 10^{-5}\,\mathrm{nA/V}^2$ and $D_0 = 1.895 \pm 0.012 \times 10^3\,\mathrm{V}$. For this set of parameters A_0, B_0, C_0 and D_0, equation (3) can be numerically solved to find the expected value of ΔV as a function of V_{DC}. The results are shown in Fig. 3 (solid lines) alongside the direct measured values (I and ΔV versus V_{DC}) and in Fig. 5 in reduced coordinates. They agree well with the measurements for both the current I and voltage drop ΔV versus V_{DC}. Little discrepancies are visible in Fig. 5, which could be due to variations in the value of the beta factor, which are not taken into account in Eq. 2. The plots we present here seem to differ from other results in diamond [10] or semiconductors [30, 31] where strong saturations of the FN plots are observed. This is partly due to the fact that in these cases, larger values of applied voltage are used spanning over regions with more different physical behaviours.

From the values of parameters B_0 and D_0 we can retrieve numerical values for some of the physical parameters of the diamond tip. The Poole-Frenkel mechanism leads to a current I that scales as

$$I \propto \Delta V \exp\left(\frac{\sqrt{\frac{e^3\Delta V}{\pi\epsilon_0\epsilon_r d}} - E_a}{k_B T}\right) \qquad (4)$$

where ϵ_r is the relative permittivity of diamond, d is the field penetration length inside the diamond, k_B the Boltzmann constant, T the temperature, and E_a an activation energy (or trap energy) that is related to the trap potential of impurities inside the diamond. This means $B_0 = \sqrt{\frac{e^3}{\pi\epsilon_0\epsilon_r d}}/k_B T$. E_a has been measured for diamond needles in [10] and is on the order of 0.2 eV. In diamond films, earlier studies reported similar values for the trap energy [5, 8]. The value of B_0 given by the fit leads to $\epsilon_r d = 170\,\mu\mathrm{m}$ and taking the bulk value for the relative permittivity of diamond $\epsilon_r = 5.7$ gives $d = 30\,\mu\mathrm{m}$. The SEM images show the diamond nanotip is about $70\,\mu\mathrm{m}$ long, but its surface can be partially covered by carbon amorphous conductive layers.

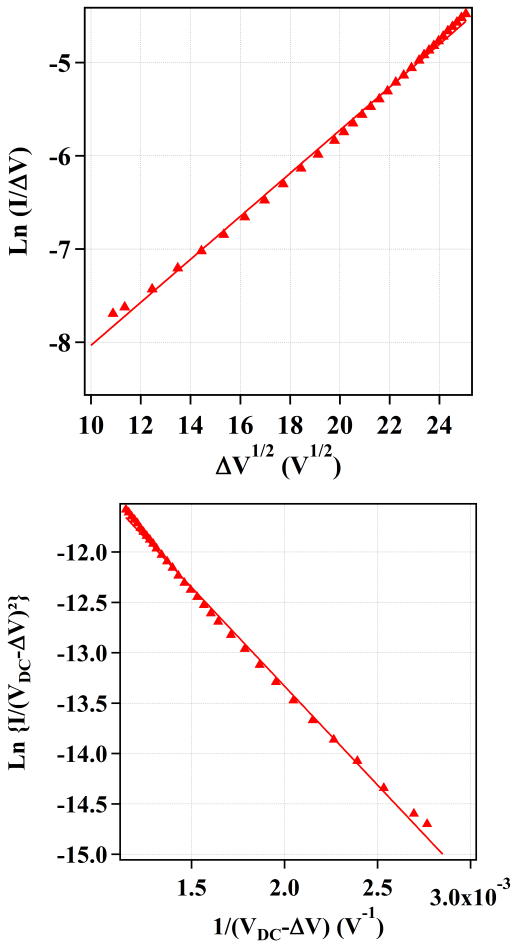

FIG. 5: Top: Poole-Frenkel plot of the measured current as a function of the potential difference ΔV between both ends of the diamond tip. The solid line represent the curve obtained for the combined fit of I and ΔV versus V_{DC}. Bottom: the same current is plotted as a function of $V_{\mathrm{DC}} - \Delta V$ which corresponds to the electric field at the diamond-vacuum junction.

On the other hand, the Fowler-Nordheim parameter D is equal to $\frac{4\sqrt{2m}}{3\hbar e}\phi^{3/2}\,v(y)\,\frac{1}{\beta}$ with m the electron mass, ϕ the workfunction and $v(y)$ a slowly varying special mathematical function [27] of the parameter $y = \sqrt{\frac{e^3\beta(V_{\mathrm{DC}}-\Delta V)}{4\pi\epsilon_0}}/\phi$. Many modern experimental papers on field emission use a simplified form in which the factor $v(y)$ does not appear. This is equivalent to taking $v(y) = 1$, and causes error in the current density prediction by a factor of 100. Here we use the value $v(w) = 0.6$, which is similar to the value used for a metallic field emitter [32]. Taking $D = D_0 = 1895\,\mathrm{V}$ from the fit and a workfunction ϕ of 5 eV (from [7] for instance), we get $\beta = 2.4 \times 10^7\,\mathrm{m}^{-1}$. The value of beta can also be estimated from the geometry of the emitter. In the first

approximation it depends only on the radius of the emitter r as $\beta = 1/(kr)$ with the coefficient k approximately equal to 5 [33]. From the SEM image, we got $r = 25$ nm and $\beta = 0.8 \times 10^7\,\mathrm{m}^{-1}$ which is much lower than the value obtained from FN plot fit. The discrepancy can be explained by the fact that within our voltage range, the current is saturated due to the field penetration effect. In [10], it was shown that at smaller currents where there is no saturation the I-V curve in FN plot bends downward i.e. its slope becomes higher. This means that β, estimated from the fit of FN plot, will be smaller in this region and should be closer to its value determined from the geometry of the emitter.

In our experiments, the linear dependence of the voltage drop with a slope of 0.53 shows that with an applied voltage V_{DC} between 500 and 1500 V, the current limitation is rather balanced between the PF and the FN mechanisms, both contributing to current limitation with differential resistances of the same order. This differential resistances can be defined as

$$R_{PF} = \Delta V/I = 1/Ae^{-B\sqrt{\Delta V}}$$

and

$$R_{FN} = (V_{\mathrm{DC}} - \Delta V)/I = \frac{1}{C(V_{\mathrm{DC}} - \Delta V)} e^{\frac{D}{V_{\mathrm{DC}} - \Delta V}}$$

Fig. 6 shows the voltage divider as a function of the applied voltage V_{DC}. It is indeed almost constant for an applied voltage between 1000 V and 2000 V.

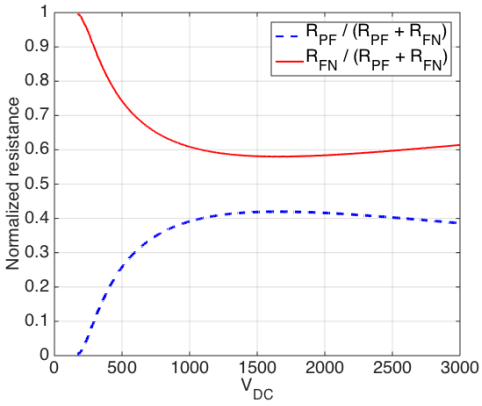

FIG. 6: Normalized resistances (voltage divider)of Poole-Frenkel and Fowler-Nordheim $R_{PF}/(R_{PF} + R_{FN})$ and $R_{FN}/(R_{PF} + R_{FN})$ calculated from I and ΔV as a function of V_{DC}.

However, the behavior is different for other values of V_{DC}. At low applied voltage, the voltage drop is close to zero, meaning that the PF conduction in the tip is not relevant and the PF resistance is much smaller than the FN resistance. At higher V_{DC} (above 2000 V for our parameters) numerical calculations shown in Fig. 6 show that the PF resistance decreases slower, indicating that the FN mechanism is taking over again.

V. INFLUENCE OF THE EXPERIMENTAL PARAMETERS ON THE VOLTAGE DROP

From this model, it is clear that modifying the diamond tip parameters will change the values of the four relevant parameters A, B, C and D and will modify the balance between the PF and FN mechanisms. This can be observed either in the current or the voltage drop dependence on the applied voltage. Experiments performed in [10] showed that the PF mechanism is indeed affected by temperature through a modification of the B parameter. We were not able to reproduce these experiments that require the tip to be cooled down or heated by several hundreds of Kelvin. However, our model shows that this would translate into a modification of the slope of the linear part of the voltage drop dependence. This variation is shown in Fig. 7 (left) where the voltage drop and the slope are plotted for various values of the B parameter. As expected, at high temperature, the PF mechanism is dominant for higher voltage, since the associated resistance is very low.

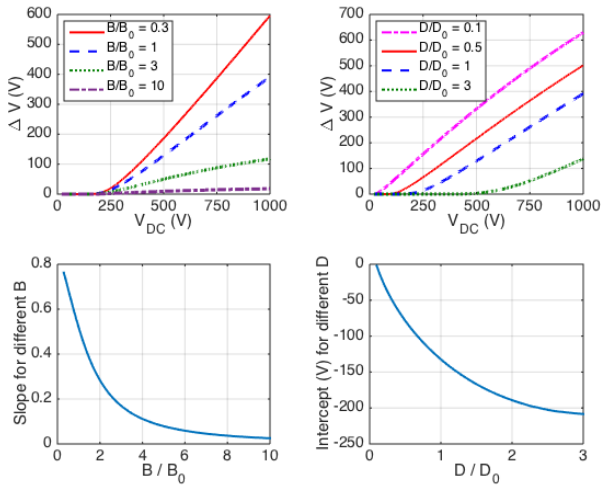

FIG. 7: Evolution of the Voltage drop as a function of the applied voltage for different values of the parameters B and D. Top left is a series of plots of ΔV vs V_{DC} for values of B ranging from $0.3 * B_0$ to $10B_0$. Bottom left shows the slope of the linear dependence of ΔV as a function of B/B_0. Top right is a series of plots of ΔV vs V_{DC} for values of D ranging from $0.1 * B_0$ to $3B_0$. Bottom right shows the vertical intercept of the linear dependence of ΔV as a function of D/D_0.

A similar interpretation can be made for the influence of the D parameter. Calculations of ΔV for various values of D is shown in Fig. 7 (right). For a single diamond tip, the value of D cannot be modified easily since it depends on the tip shape and material. However, laser illumination can lead to an increase in the emission current by various physical mechanisms, which is equivalent to a reduction of the FN differential resistance. This

experiment has been performed with femtosecond pulses (300 fs duration, 1030 nm wavelength, 1 MHz repetition rate) and a focal spot of a few micrometres on the apex of the biased diamond tip. This experiment differs from what has been studied by Porshyn et al. [16] and Borz et al. [34]. The main difference is that in our experiment, only the apex is illuminated thanks to a very tight laser focus. This means that the PF conduction inside the diamond is not affected, and only the emission process at the apex is modified. We observed a transition in the emission regime when the laser power is increased. The voltage drop changes when passing through a critical

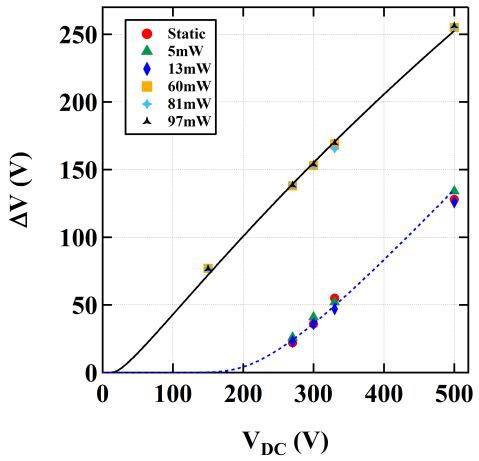

FIG. 8: Measurement of ΔV as a function of V for DC and DC+laser field emission for different laser powers (corresponding to different shaped symbols). Above a critical laser power, the voltage drop changes, following a linear behavior versus applied voltage $V_{\rm DC}$, with a similar slope compared to the static emission, but with a different intercept, close to zero. The lines correspond to two different fits which gives different values of the D parameter.

laser power of about 50 mW as shown in Fig. 8. Below the critical power, the voltage drop behaves as it would without laser illumination. Above it, the voltage drop increases linearly with $V_{\rm DC}$ with an intercept close to 0. This decreases the parameter D and therefore the FN resistance. Fitting the ΔV versus $V_{\rm DC}$ under laser illumination gives a new value of the D parameter, which drops to 73 V, which is more than twenty times smaller than the value obtained in static measurements. The fit is however not as precise and also shows that the decrease of D is associated with a decrease of the C parameter as well. If we assume that the D parameter can still be written as $\frac{4\sqrt{2m}}{3\hbar e}\phi^{3/2}\,v(y)\,\frac{1}{\beta}$, then the drop of D can be a consequence of a change in either the workfunction ϕ, the voltage-to-field factor β or even the $v(y)$ function. A more precise interpretation of these findings requires essentially a microscopic analysis which is out of the scope of the present study and requires intensive investigations which are in progress now.

VI. CONCLUSION

In conclusion, we have presented experimental measurements of current and voltage drop versus $V_{\rm DC}$ in diamond nanoemitters acting as a point electron source in vacuum. We confronted these measurements to a macroscopic electrical model, that is able to accurately fit the data, including the linear dependence of the voltage drop with a negative intercept. This model combines Poole-Frenkel conduction and Fowler-Nordheim tunneling which are both contributing to the measured current and voltage drop. We showed how laser illumination on the tip apex only can shift up the voltage drop and keep the slope constant. This study also explains how using the reduced voltage at the apex $V_{\rm DC} - \Delta V$, the Fowler-Nordheim plots show much less saturation than with regular coordinates. From this work onward, it becomes necessary to carry out further investigations to reveal in more details the microscopic mechanisms so that it becomes possible to optimize samples and experimental conditions to obtain results which may be greatly attractive for both applied and fundamental perspectives.

ACKNOWLEDGMENTS

This work was supported by Programme Investissements d'Avenir under the programs ANR-11-IDEX-0002-02, reference ANR-10-LABX-0037-NEXT, ANR-13-BS04-0007-01 and ANR-10-LABX-09-01, LabEx EMC3, by the European Union with the European Regional Development Fund (ERDF) and the Regional Council of Normandie. ANO and VIK are grateful for financial support from Russian Foundation for Basic Research (grant #18-29-19071).

[1] C. Wang, A. Garcia, D. C. Ingram, M. Lake, and M. E. Kordesch, Electronics Letters **27**, 1459 (1991).
[2] K. Okano, S. Koizumi, S. R. P. Silva, and G. A. J. Amaratunga, Nature **381**, 140 (1996).
[3] C. Bandis and B. B. Pate, Applied Physics Letters **69**, 366 (1998).
[4] M. W. Geis, J. C. Twichell, N. N. Efremow, K. Krohn, and T. M. Lyszczarz, Applied Physics Letters **68**, 2294 (1998).
[5] J. W. Glesener and A. A. Morrish, Applied Physics Letters **69**, 785 (1998).

[6] W. Zhu, G. P. Kochanski, and S. Jin, Science (New York, N.Y.) **282**, 1471 (1998).

[7] O. Gröning, O. M. Küttel, P. Gröning, and L. Schlapbach, Journal of Vacuum Science & Technology B: Microelectronics and Nanometer Structures Processing, Measurement, and Phenomena **17**, 1970 (1999).

[8] A. Göhl, B. Günther, T. Habermann, G. Müller, M. Schreck, K. H. Thürer, and B. Stritzker, Journal of Vacuum Science & Technology B: Microelectronics and Nanometer Structures Processing, Measurement, and Phenomena **18**, 1031 (2000).

[9] Z. Wang, Q. Wang, H. Li, J. Li, P. Xu, Q. Luo, A. Jin, H. Yang, and C. Gu, Science and Technology of Advanced Materials **6**, 799 (2005).

[10] V. I. Kleshch, S. T. Purcell, and A. N. Obraztsov, Scientific Reports **6**, 35260 (2016).

[11] J. R. Arthur, Journal of Applied Physics **36**, 3221 (1965).

[12] L. Apker and E. Taft, Physical Review **88**, 1037 (1952).

[13] R. G. Forbes, Applied Physics Letters **110**, 133109 (2017).

[14] A. N. Obraztsov, P. G. Kopylov, B. A. Loginov, M. A. Dolganov, R. R. Ismagilov, and N. V. Savenko, Review of Scientific Instruments **81**, 013703 (2010).

[15] A. S. Orekhov, F. T. Tuyakova, E. A. Obraztsova, A. B. Loginov, A. L. Chuvilin, and A. N. Obraztsov, Nanotechnology **27**, 455707 (2016).

[16] V. Porshyn, V. I. Kleshch, E. A. Obraztsova, A. L. Chuvilin, D. Lützenkirchen-Hecht, and A. N. Obraztsov, Applied Physics Letters **110**, 182101 (2017).

[17] F. T. Tuyakova, E. A. Obraztsova, E. V. Korostylev, D. V. Klinov, K. A. Prusakov, A. A. Alekseev, R. R. Ismagilov, and A. N. Obraztsov, Journal of Luminescence **179**, 539 (2016).

[18] L. Rigutti, L. Venturi, J. Houard, A. Normand, E. P. Silaeva, M. Borz, S. A. Malykhin, A. N. Obraztsov, and A. Vella, Nano Letters **17**, 7401 (2017).

[19] S. A. Malykhin, R. R. Ismagilov, F. T. Tuyakova, E. A. Obraztsova, P. V. Fedotov, A. Ermakova, P. Siyushev, K. G. Katamadze, F. Jelezko, Y. P. Rakovich, and A. N. Obraztsov, Optical Materials **75**, 49 (2018).

[20] S. A. Malykhin, J. Houard, R. R. Ismagilov, A. S. Orekhov, A. Vella, and A. N. Obraztsov, physica status solidi (b) **255**, 1700189 (2018).

[21] M. R. Bionta, B. Chalopin, J. P. Champeaux, S. Faure, A. Masseboeuf, P. Moretto-Capelle, and B. Chatel, Journal of Modern Optics **61**, 833 (2014).

[22] M. Bionta, S. Weber, I. Blum, J. Mauchain, B. Chatel, and B. Chalopin, New Journal of Physics **18**, 103010 (2016).

[23] J. Frenkel, Physical Review **54**, 647 (1938).

[24] K. X. Liu, C.-J. Chiang, and J. P. Heritage, Journal of Applied Physics **99**, 034502 (2006).

[25] M. Choueib, A. Ayari, P. Vincent, S. Perisanu, and S. T. Purcell, Journal of Applied Physics **109**, 073709 (2011).

[26] R. H. Fowler and L. Nordheim, Proceedings of the Royal Society A: Mathematical, Physical and Engineering Sciences **119**, 173 (1928).

[27] E. L. Murphy and R. H. Good, Physical Review **102**, 1464 (1956).

[28] R. G. Forbes and J. H. Deane, Proceedings of the Royal Society A: Mathematical, Physical and Engineering Sciences **463**, 2907 (2007).

[29] G. Fursey, Applied Surface Science **94-95**, 44 (1996).

[30] L. M. Baskin, O. I. Lvov, and G. N. Fursey, Physica Status Solidi (b) **47**, 49 (1971).

[31] M. Choueib, A. Ayari, P. Vincent, M. Bechelany, D. Cornu, and S. T. Purcell, Physical Review B **79**, 075421 (2009).

[32] R. G. Forbes, Journal of Vacuum Science & Technology B: Microelectronics and Nanometer Structures **26**, 209 (2008).

[33] R. Gomer, Field emission and field ionization, Vol. 34 (Harvard University Press Cambridge, MA, 1961).

[34] M. Borz, I. Blum, A. Vella, O. Torresin, J. Mauchain, B. Chalopin, and A. N. Obraztsov, in 2017 30th International Vacuum Nanoelectronics Conference (IVNC) (IEEE, 2017) pp. 86–87.